SusMat

WILEY

SusMat

RESEARCH ARTICLE OPEN ACCESS

Sustainable Photochromic Wearables With Excellent Retention and Superior Stability for Customizable Patterns and Information Security Encryption

Junze Zhang | Xinlong Liu | Tiandi Chen | Jing Han | Taosif Ahmed | Xin Wang | Qian Wang | Cuiqin Fang | Bingang Xu

Nanotechnology Center, School of Fashion and Textiles, The Hong Kong Polytechnic University, Kowloon, Hong Kong, China

Correspondence: Bingang Xu (tcxubg@polyu.edu.hk)

Received: 15 February 2025 | **Revised:** 29 April 2025 | **Accepted:** 14 May 2025

Funding: This work was supported by the Innovation and Technology Commission of the Government of the Hong Kong Special Administrative Region (Project No. ITS/139/21), and J. Zhang would like to thank The Hong Kong Polytechnic University for providing him with a postgraduate scholarship.

Keywords: color retention | customizable patterns | MoO_3 | photochromic wearables | stability

ABSTRACT

Advanced photochromic wearables have aroused growing research interest in customizable pattern display, information security encryption, and intelligent fabrics. Molybdenum trioxide (MoO_3), distinguished by its superior photochromic capabilities, has emerged as a prime contender for photochromic wearables among several photochromic materials. However, the advancement of rewritable wearables with MoO_3 is constrained by inadequate adhesion, insufficient stability, and limited scalability. Herein, a fiber-based photochromic wearable is designed and developed by covalently bonding MoO_3 microcapsules (MM) nanoparticles with a sheath-core structure into pristine cotton fabrics and integrating MM nanoparticles with sodium alginate (SA) through electrostatic forces and peptide linkages. The resulting photochromic wearable exhibits reversible color transformation and exceptional photochromic characteristics, including remarkable fatigue resistance (>40 cycles), rapid light response, and outstanding color retention (>60 days). Moreover, the photochromic wearable exhibits exceptional stability in diverse harsh environments, including different acid-base solutions (pH 2.0–9.0), various temperatures (−30°C–60°C), indoor light and sunshine exposure, and repeated laundering (>15 cycles). This photochromic fabric exhibits exceptional wearability, boasting remarkable flexibility (17 mm) and biocompatibility (cell viability >95%). Notably, rewritable T-shirts and QR code information security encryption systems are demonstrated, highlighting their potential in customizable designs, flexible rewritable textiles, and information security encryption.

1 | Introduction

The growing need for aesthetics, customization, and diverse textiles has propelled advancements in fiber-based wearables, including stimuli-switching devices, thermal-regulated textiles, wearable sensors, and antibacterial fabrics [1–7]. Consumers will discard and replace conventional garments featuring static patterns after repeated use because of their monotonous, immutable, and antiquated designs. This has led to the release of a massive amount of chemicals and human living products into the environment, escalating manufacturing costs and pollution. Fiber-based photochromic wearables are considered optimal for reducing costs and addressing environmental issues owing to their excellent light responsiveness, favorable fatigue

resistance and reversibility, and diverse functionalities [8–10]. These wearables provide individuals with personalized options while demonstrating boundless inventiveness and potential in the convergence of technology and fashion.

A photochromic wearable that utilizes photochromic materials can switch its colors by the reversible transformation of photochromic materials between two states [11–13]. These wearables demonstrate considerable potential in optical data storage/recording, customizable patterns, photonic memory, ink-free printing, information security encryption, and optoelectronic devices [14–17]. Currently, the research on photochromic wearables mostly focuses on improving their light response speed, color change intensity, and reversibility. Nevertheless, it is still a considerable challenge to develop fiber-based photochromic fabrics with great scalability, long color retention, and excellent environmental stability in the face of the complex manufacturing process and inevitable environmental changes. Great scalability can markedly decrease manufacturing expenses, accelerate production processes, and improve the commercialization of production. Furthermore, longer color retention guarantees that the designs on photochromic wearables remain clear and visible after prolonged use, making them suitable for everyday wear. Excellent environmental stability enables photochromic wearables to keep stable photochromic performance despite fluctuations in the surrounding environment. Improving the commercialization and dissemination of photochromic textiles for attractive applications necessitates that these materials swiftly display distinct patterns, retain them for an extended period, and enable a rapid writing–erasing cycle for information transformation. Therefore, it is essential to develop scalable photochromic wearables with excellent color retention and extraordinary environmental stability for customizable patterns and information security encryption applications.

Photochromic materials, including organic materials, such as spiropyran, spirooxazine, and diarylethene; transition metal oxides, such as titanium dioxide, tungsten trioxide, and molybdenum trioxide (MoO_3); and polyoxometalates [11, 18–21], have been incorporated into fiber-based photochromic wearables for sustainable applications. MoO_3 is a multifaceted *n*-type semiconductor with potential applications in photochromic and electrochromic systems, electronics, catalysis, sensors, energy storage devices, and superconductors [22, 23]. MoO_3 demonstrates excellent reversibility, rapid color transitions, high fatigue resistance and durability, and long color retention [23, 24], making it an exemplary option for photochromic wearables. However, the advancement of rewritable wearables based on MoO_3 continues to pose a significant barrier. When photochromic materials are incorporated into the fabric substrate through physical stress or weak interaction, it eventually leads to the degradation of the stability, durability, and photochromic functionality of photochromic fabrics after prolonged wear. In addition, the detergent (pH > 8) used in the washing process will neutralize MoO_3, which will completely eliminate its photochromic properties. By putting photochromic materials inside microcapsules, sensitive substances can be physically enclosed in a protective matrix or wall material. This protects the core materials from reactive and corrosive environments, resulting in better durability, fatigue resistance, and photochromic performance. Chitosan, a nitrogen-containing polysaccharide, has garnered significant interest in biomedicine, water treatment, cosmetics, the food industry, the textile industry, and agriculture owing to its inherent nontoxicity, biodegradability, biocompatibility, and antimicrobial properties [25–27]. Chitosan is a natural polymer that can be used as the wall of microcapsules. Its amino (NH_2) and hydroxyl (OH) groups help it stick strongly to textiles by reacting and coordinating with them. In addition, when a cross-linking agent is added to chitosan and nanoparticles, they can form a shell-core structure that effectively encloses the nanoparticles within the chitosan [28, 29]. Also, anions in sodium alginate (SA) can interact with cations in chitosan through electrostatic adsorption, bringing more protection for MoO_3 nanoparticles even against damage from the outside. Therefore, it is important to develop a photochromic fabric with MoO_3 microcapsules (MM) nanoparticles that can keep its photochromic properties even after being washed many times and exposed to different environmental conditions.

Herein, we have designed and developed long-retention-time and highly environmental stability photochromic wearables utilizing MoO_3 for customizable patterns and information security encryption. The MM nanoparticles, characterized by a sheath-core structure, are integrated into cotton fabrics using covalent grafting, and then $-NH^{3+}$ on the surface of MM nanoparticles attracts the —COOH in the SA through electrostatic forces and dehydration reactions to develop photochromic wearables. The photochromic wearable shows great reversible "writing–erasing" capability (>30 cycles), fast light response (color saturation with a UV dose of 48 kJ m^{-2}), and outstanding color retention capability (>60 days). Additionally, this photochromic wearable has excellent environmental stability in avoiding the corrosion of repeated washing (15 cycles), various pH (pH 2.0–9.0), and temperature (−30°C–60°C) environments, benefiting from the tight encapsulation of chitosan and SA. Moreover, this photochromic fabric maintains a distinct pattern under both indoor and sunlight exposure and exhibits great biocompatibility (cell viability > 95%), indicating its suitability for daily use and athletic activities. As an application, a rewritable T-shirt and a QR code information security encryption system are demonstrated to validate the feasibility of the practical applications in customizable patterns and information security encryption. This study provides insights into the design and manufacture of scalable, long-color-retention, and environment-stable MoO_3-based wearable photochromic wearables, paving the way for realizing tremendous advancement in sustainable and smart textiles.

2 | Results and Discussion

Figure 1A exhibits the fabrication procedure of SA/MM/Epoxy pristine cotton fabrics (SAME-PCFs) employing the microcapsule technique, covalent grafting, and dehydration reactions. Initially, the PCFs were subject to NaOH solution treatment to eliminate oils and impurities, hence augmenting the presence of supplementary functional groups on the fiber surface. Subsequently, the PCFs were modified using Glycidoxypropyltrimethoxysilane (KH560) to introduce epoxy groups onto the cotton fiber surface, resulting in Epoxy PCFs (E-PCFs). Next, E-PCFs were submerged in an MM nanoparticle solution, facilitating covalent interaction between E-PCFs and MM nanoparticles, hence resulting in the formation of MM/epoxy PCFs (ME-PCFs). Ultimately, SAME-PCFs were attained by integrating ME-PCFs

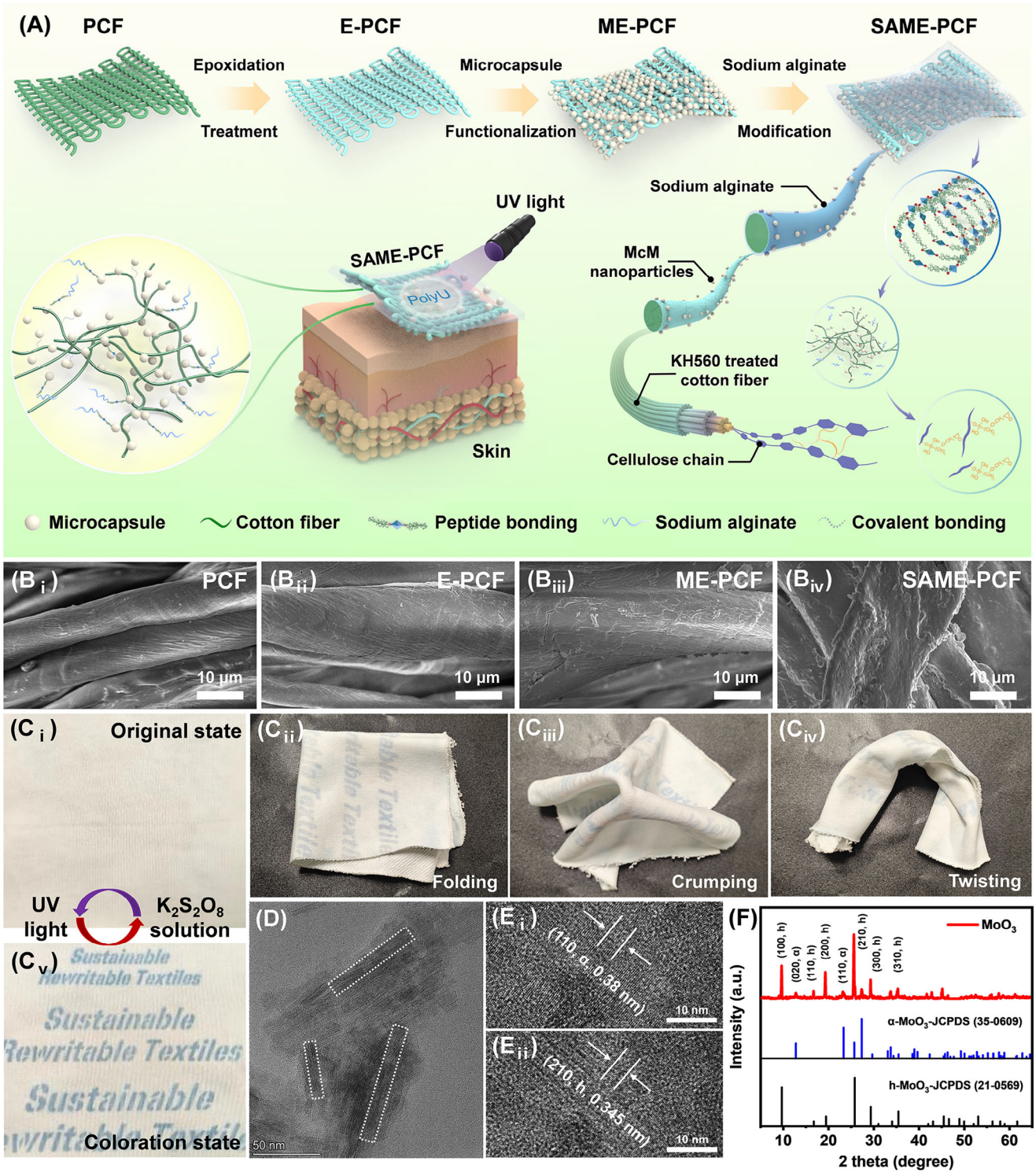

FIGURE 1 | The fabrication of SAME-PCFs and characterization of MoO_3 nanoparticles and SAME-PCFs. (A) Schematic diagram of a procedure for preparing SAME-PCFs. (B_1–B_4) Surface morphology of PCF SAME-PCFs. (C_i–C_v) Images of the SAME-PCFs in different states (original state, folding state, crumping state, twisting state, and coloration state). (D) TEM images of the prepared MoO_3 nanoparticles. (E_i–E_{ii}) High-resolution TEM images of the MoO_3 nanoparticles. (F) XRD patterns of the prepared MoO_3 nanoparticles.

with SA via electrostatic interactions and dehydration processes. The comprehensive materials and manufacturing methods are detailed in the experimental section. The SEM pictures of PCF, E-PCF, ME-PCF, and SAME-PCF were presented to illustrate alterations in fiber surface morphology. Figure $1B_i$ illustrates the distinctive wrinkling and scale architecture of the PCF's surface. After being treated with KH560, the cotton fiber surface attains a smooth texture with uniform folds (Figure $1B_{ii}$), showing successful modification of KH560. After the treatment with the MM nanoparticles, the ME-PCF surface exhibits increased roughness and a scaly texture akin to that of MoO_3 nanoparticles (Figure $1B_{iii}$), demonstrating the successful covalent grafting of

MM nanoparticles. Figure 1B$_{iv}$ displays a rougher cotton fiber surface, attributable to the tight adsorption of SA on the fiber surface. Figure S1 offers a comprehensive depiction via SEM images at different magnifications to corroborate the previously reported findings. Figure 1C$_i$–C$_{iv}$ illustrates the SAME-PCFs under various deformations (i.e., original, folding, crumpling, and twisting), demonstrating their remarkable flexibility and ease of integration into everyday fabrics. Figure 1C$_v$ shows the capability of SAME-PCFs to create and eliminate customizable patterns under UV light exposure and potassium persulfate ($K_2S_2O_8$) solution.

The morphology and structure of MoO_3 nanoparticles underwent further characterization. TEM images indicate that the synthesized MoO_3 nanoparticles' predominant morphological structure comprises nanosheets (Figure 1D; Figure S2a–d). The nanosheet particles exhibit lengths between 50 and 100 nm, widths between 10 and 15 nm, and aspect ratios from 3.33 to 10. Hydrothermal synthesis of MoO_3 nanoparticles is depicted in Figure S3, which primarily comprises the nucleation and development of the MoO_3 nanoflakes and the formation of secondary nanoflakes through directed aggregation of the primary nanoflakes. Figure 1E$_i$,E$_{ii}$ present high-resolution TEM pictures that demonstrate the lattice plane distances of 0.38 and 0.345 nm. These measurements pertain to the crystal plane in MoO_3 nanoparticles, indexed as (1 1 0, α) and (2 1 0, h). Figure S4 depicts the size distribution of the MoO_3 nanoparticles, indicating a primary size range of 60 to 250 nm, consistent with the TEM images. The nanosheet and small-sized MoO_3 nanoparticles can be more easily combined with fibers along their surfaces, enhancing bonding strength and improving photochromic properties. According to the standard powder diffraction files JCPDS 21–0569 and 35–0609, Figure 1F illustrates that the diffraction peak results from both the hexagonal phase (h-MoO_3) and the orthogonal crystal phase (α-MoO_3) of MoO_3. The hexagonal and orthogonal phases of MoO_3 have a narrower band gap and smaller band gap energy, which promotes the separation of electrons and positive holes and provides an enhanced way for the diffusion of photoprotons, resulting in a better photochromic effect of MoO_3.[30, 31].

We further assessed the binding mechanism in the manufacture of SAME-PCFs (Figure 2A). During the epoxidation treatment, KH560 easily hydrolyzes in water and converts alkyl siloxane into silanol. The cotton fabric, consisting of cellulose, is abundant in positively charged functional groups, such as OH groups. The silanol in KH560 reacts directly with OH groups on the cotton fiber surface, leaving the epoxy groups on the surface of PCF exposed, creating the E-PCF (chemical reaction i). In the chemical reaction ii, MoO_3 nanoparticles cross-link with the NH_2 group on the surface of the chitosan and the aldehyde group of glutaraldehyde (GA) solution, leading to the formation of the MM nanoparticles with a shell-core structure. In the subsequent step iii, a nucleophilic addition reaction takes place, and strong covalent bonds are made between the —NH^{3+} groups on the shell of the MM nanoparticles (at pH 5) and epoxy groups on the surface of E-PCF. Robust covalent bonding can guarantee the stability and durability of the MM nanoparticles on the ME-PCF's surface. In the chemical reaction iv, the —NH^{2+} on the wall material of the microcapsule is converted into —NH^{3+}, and the carboxyl group in the SA molecule remains as —COOH at pH 5. The extra —NH^{3+} on the surface of MM nanoparticles attracts the —COOH in SA through electrostatic force and dehydration reaction, and the SAME-PCFs are obtained.

Figure 2B shows how the UV–vis absorbance of SAME-PCFs changed after going through different pad-dyeing cycles. When the concentration of MM nanoparticles is 10 mg mL^{-1}, the absorbance of SAME-PCF is about 0.89. It goes up to about 1.23 when the number of pad-dyeing cycles goes from 1 to 3. Afterwards, the absorbance only attains around 1.28 as the pad-dyeing cycles rise from 3 to 5. We also evaluated the effect of concentration on the photochromic performance of SAME-PCFs subject to 3 pad-dyeing cycles (Figure 2C). The absorbance of the SAME-PCFs increases from around 0.4 to 1.23 as the concentration of MM nanoparticles escalates from 2 to 10 mg mL^{-1}. Thereafter, the absorbance gradually increases to about 1.30 at a concentration of 15 mg mL^{-1}. Given the procedure's complexity and efficiency, the SAME-PCF subject to 3 pad-dyeing cycle iterations at a concentration of 10 mg mL^{-1} was selected for future investigation. Figure 2D illustrates that the PCF and E-PCF exhibit greater flexibility, measuring 13.7 and 11 mm, respectively. Following the alteration of cotton fibers with MM nanoparticles and SA, they retain remarkable flexibility, measuring approximately 16.7 and 17.3 mm. The superior flexibility ensures that the photochromic wearables conform closely to the intricate deformations of the human body. Upon irradiation with UV light (λ = 365 nm), all the photochromic textiles progressively transitioned to blue (Figure 2E). However, SAME-PCFs treated with 10% MM nanoparticles show a stronger photochromic reaction when exposed to the same UV light as SAME-PCFs treated with 2% and 5% concentrations of MM nanoparticles. Cytotoxicity and skin allergy tests confirmed the excellent biocompatibility of SAME-PCFs, which are crucial for daily use safety, human skin protection, and sustainable and eco-friendly development. Figure 2F illustrates that SAME-PCFs maintain a cell vitality of approximately 99% (>80%) after 5 days, which is equivalent to the viability of PCFs (93%). Figure S5 illustrates the optical density (OD) values of the PCF, SAME-PCFs, and control, indicating a gradual increase in OD values over time. Furthermore, the findings of the skin allergic reaction test demonstrated that SAME-PCF is non-harmful to the skin (Figure S6). One can directly apply it to the skin without any additional treatment, and it continues to be nonirritating even after 72 h of application. These demonstrate that the SAME-PCF, possessing superior biocompatibility, satisfies the criteria for wear safety and prevents harm to human skin.

Figure 3A illustrates the mechanical properties of the PCF, E-PCF, ME-PCF, and SAME-PCF. The application of MM nanoparticles and SA enhances breaking strength, elongation, and modulus. The PCF and E-PCF exhibit breaking strengths of around 131.5 and 155 N, respectively. The strength rises to approximately 181.3 N following treatment with a solution of MM nanoparticles. After the SA solution modification, the valve's force increases to roughly 204 N (as illustrated in Figure S7a). The PCF and the E-PCF exhibit initial tensile strains of around 73.7% and 79.8%, respectively. The tensile strain markedly increases with the application of MM nanoparticles and SA coating, attaining approximately 96.7% and 109.1%, respectively (Figure S7b). The incorporation of MM nanoparticles with high mechanical strength and SA enhances the connection between fibers. Meanwhile, the robust covalent connection between the negatively

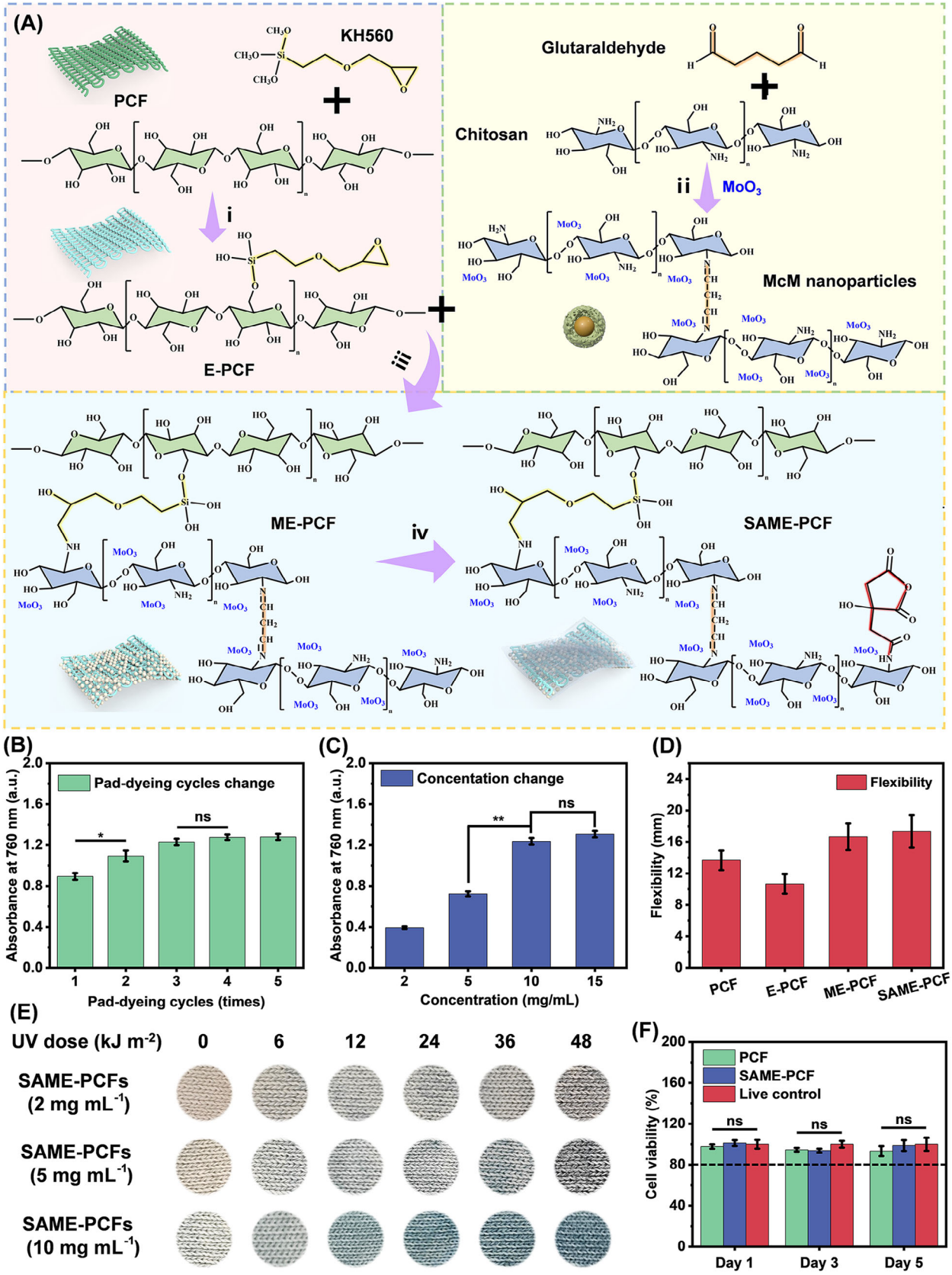

FIGURE 2 | The binding mechanism and performance of the photochromic fabrics. (A) The bonding mechanism for fabricating SAME-PCFs. (B) Photographs of SAME-PCFs with different MM nanoparticle concentrations. (C) The absorbance changes of the SAME-PCFs with increasing pad-dyeing cycles. (D) The absorbance changes of the SAME-PCFs with increasing concentration of MM nanoparticles. (E) The change in flexibility for preparing SAME-PCFs. (F) Cell viability for the PCF, SAME-PCFs, and control after 1, 3, and 5 days of incubation.

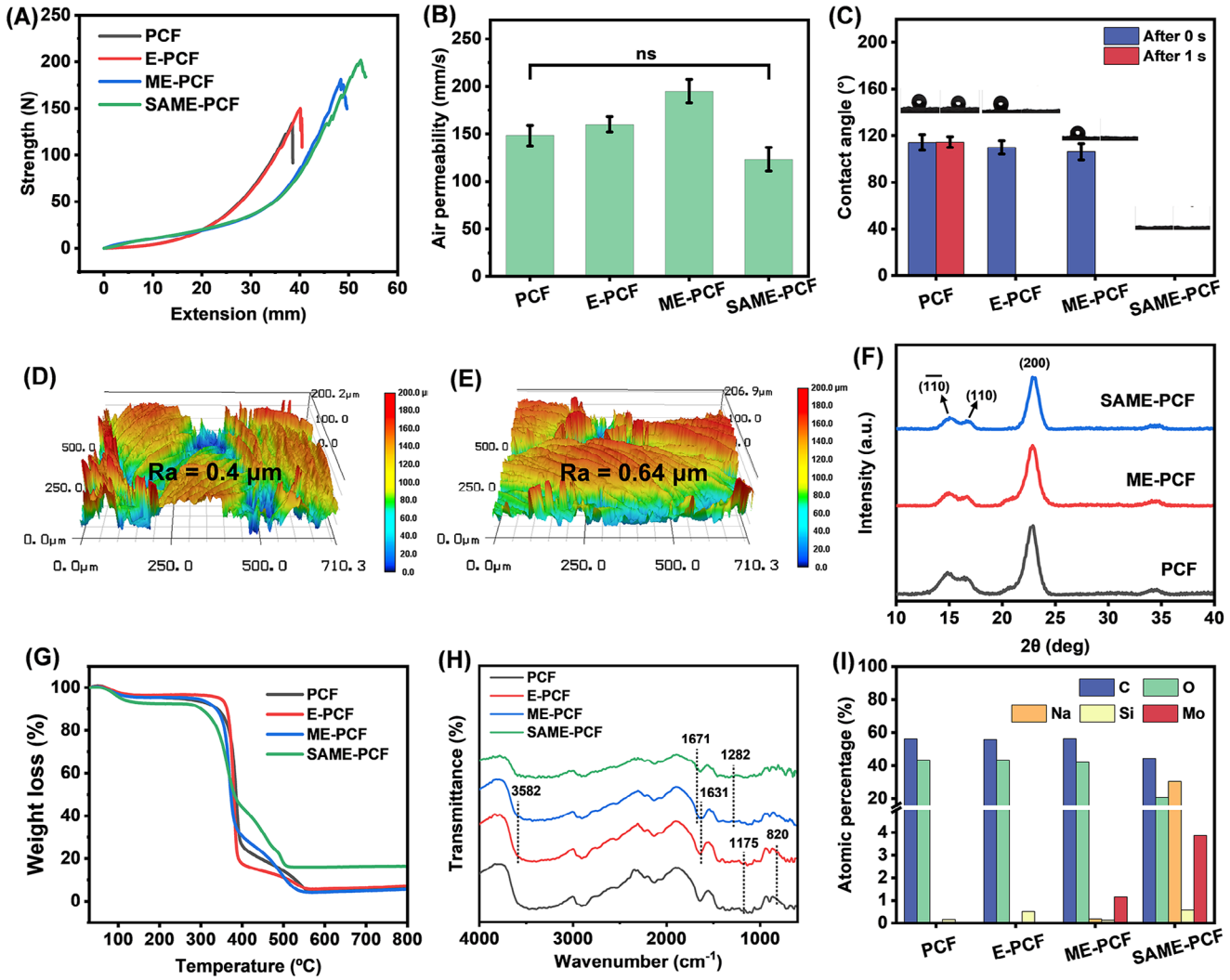

FIGURE 3 | Characterization of the MoO_3 nanoparticles and fabrics. (A) The tensile strain of the PCF, E-PCF, ME-PCF, and SAME-PCF. (B) Air permeability of cotton fabrics before and after treatment. (C) Contact angle of the cotton fabrics before and after functionalization. (D) Surface roughness of the PCF. (E) Surface roughness of the SAME-PCF. (F) x-Ray diffraction profile of PCF, ME-PCF, and SAME-PCF. (G) Thermal stability of the cotton fabrics before and after modification. (H) FT-IR spectra of the PCF, E-PCF, ME-PCF, and SAME-PCF. (I) Element content of the cotton fabrics before and after functionalization.

charged components of the MM nanoparticles and the positively charged functional groups of the cotton fiber substantially enhances the mechanical properties of the fabric. We evaluated and examined the air permeability of cotton fabrics prior to and during functionalization, as shown in Figure S8a–d. Figure 3B shows that the PCF has exceptional air permeability, with an air resistance of about 148 mm s^{-1}. After treatment with KH560 and MM nanoparticle solution, the air permeability rises to approximately 160 and 195 mm s^{-1}, respectively. Following SA modification, the air permeability of the SAME-PCF exhibits a minor reduction to roughly 123.3 mm s^{-1} while still maintaining a high level. The SA coating obscures some apertures in the fabric where the fibers interlace, leading to a reduction. High air permeability of SAME-PCF can facilitate the expulsion of human metabolites, including sweat and heat, into the ambient environment; hence, it preserves the comfort of photochromic fabrics throughout wear. Figure 3C illustrates the alterations in the surface hydrophilicity of these textiles as the dipping times vary. All sample contact angles exhibit 0° after 5 s (Figure S9). The PCF exhibits a contact angle of approximately 114.2° (with a dipping duration of 0 s), decreasing to roughly 108.2° after 1 s. The E-PCF and ME-PCF show contact angles of 110° and 106.3° (with a dipping duration of 0 s), rapidly decreasing to 0° after 1 s of dipping. This is due to the abundance of hydrophilic functional groups on the surface of cotton fiber, including OH and carboxyl groups. Conversely, the contact angle of SAME-PCF remains at 0° from 0 to 5 s owing to the exceptional hydrophilicity of SA. The coating of MM nanoparticles and SA retains the excellent hydrophilicity and wearing comfort of the fabric. The alteration in the surface macrostructure of samples pre- and post-functionalization is also evident through surface roughness (Figure S10). The SAME-PCF has a higher roughness (0.64 μm) than the PCF (0.4 μm) because of the presence of MM nanoparticles and SA coating (Figure 3D,E).

Additionally, SAME-PCF and ME-PCF exhibit analogous x-ray diffraction (XRD) patterns to those of PCF. This suggests that the arrangement of cellulose molecules did not change after MM

nanoparticles and SA modification (Figure 3F) [6]. Figure 3G illustrates the thermal stability of PCF, E-PCF, ME-PCF, and SAME-PCF. As the temperature rose from 30°C to 800°C, the samples experienced significant weight loss, exceeding 80%. The weight reduction noted at approximately 100°C is primarily owing to water evaporation within the fiber. At roughly 350°C, these fabrics experienced weight loss due to the decomposition of cellulose in cotton fibers. Prior to 380°C, the E-PCF demonstrates improved stability and less weight loss owing to the modification of KH560. The ME-PCF exhibits thermal degradation between 270°C and 320°C, attributable to the decomposition and oxidation of chitosan. Moreover, the incorporation of MoO_3 nanoparticles in ME-PCF and SAME-PCF leads to a reduction in both the rate and extent of weight loss at roughly 400°C. Furthermore, SAME-PCF indicates that the weight drop at 200°C is attributable to the disintegration of the SA framework, which results in the creation of an intermediate stable product. The procedure removes adjacent OH groups as water molecules. The continued oxidative breakdown of the SA carbide is responsible for the observed weight loss at a temperature of 520°C. Figure 3H shows the FT-IR spectra of cotton fabrics before and after functionalization. Characteristic peaks are observed at approximately 820, 1175, 1282, 1631, 1671, and 3582 cm^{-1}, corresponding to the bending vibrations of C—C, the asymmetric stretching vibration of Si—O—Si, the free —COO^-, the vibration of —COOH, the C═N of the Schiff base, and the stretching vibration of —NH_2, respectively. The peaks at 820 and 1175 cm^{-1} signify that KH560 has successfully adapted to PCF. The modification of MM nanoparticles induced ME-PCF, showing new peaks at 1631 and 3582 cm^{-1}, attributed to the effective cross-linking of chitosan by GA. Additionally, following the application of the SA coating, the peaks at around 1282 and 1671 cm^{-1} emerge owing to the amplification of free —COO—. The proportion of surface elements in the samples changed significantly during the photochromic functionalization process. The PCF reveals an atomic makeup of 56.35% carbon, 43.44% oxygen, 0% natrium, 0.17% silicon, and 0.04% molybdenum. The KH560 modification changes the values to 55.95%, 43.51%, 0.02%, 0.51%, and 0.01% (Figure 3I), and the increase in Si content validates the successful modification of the silane coupling agent for the PCF. Following the amalgamation of MM nanoparticles with cotton fiber, the Mo content rises to 1.16%, indicating effective microcapsule modification. After SA treatment, the Na content greatly increases to 30.41%, showing a successful combination between SA and the ME-PCF. Figure S11 illustrates the elemental distribution on the fiber, indicating a homogeneous distribution of the respective elements without any aggregation. The chemical composition and bonding states of the photochromic wearables were further investigated using x-ray photoelectron spectroscopy (XPS). Figure S12 shows the distinct peaks at 285.0, 532, 400, 231.0, 1071, and 101 eV attributed to C 1s, O 1s, N 1s, Mo 3d, Na 1s, and Si 2p, respectively. The C and O elements come from the cellulose of the PCFs, as well as the N, Mo, Na, and Si elements, which come from MM nanoparticles and SA.

The photochromic reaction and the potential photochromic mechanism of the SAME-PCF are shown in Figure 4A. Upon exposure to UV light, the SAME-PCF transitions in color from pale yellow to blue, proving that the photochromic properties of MoO_3 nanoparticles were not impacted by chitosan encapsulation. The color shift is attributable to the photochemical reduction of MM nanoparticles. Hydrogen protons participating in the reduction of Mo^{6+} likely originate from the OH groups of chitosan molecules, since chitosan tightly encapsulates MoO_3 nanoparticles. Hydrogen protons on the photochromic fabric are transferred to the metal atom Mo^{6+} via the charge transfer bridge in chitosan, leading to the reduction of Mo^{6+} to Mo^{5+} and the conversion of heteropoly blue [22, 32]. After being treated with a $K_2S_2O_8$ solution, it reverts to its original color through a reverse reaction involving electron transfer from the Mo^{5+} atom to oxygen molecules. Figure S13 illustrates the alterations in the electronic structure of the materials throughout the photochromic transformation, hence enhancing comprehension of the photochromic mechanism of the SAME-PCFs. When UV light interacts with MoO_3 nanoparticles, the photon energy exceeds the bandgap (hv > Eg). This induces the migration of electrons from the valence band to the conduction band, simultaneously generating an equivalent number of holes in the valence band. The excitation leads to the generation of electron-hole pairs, as seen in Equation (1). The SAME-PCFs, which intrinsically hold moisture inside their structure, generate the requisite protons for the photochromic reaction by the interaction of the adsorbed water with holes, as seen in Equation (2). The MoO3 nanoparticle subsequently acquires these protons, resulting in the generation of $H_xMo_x^{V}Mo_{1-x}^{VI}O_3$, as depicted in Equation (3). Simultaneously, Mo^{6+} acquires one electron from its surroundings, converting to Mo^{5+} (Equation 4). The charge transfer between the newly formed Mo^{5+} in the valence band and the adjacent Mo^{6+} in the conduction band induces a blue coloration in the MoO_3 nanoparticles (Equation 5) [22]. Upon reintroduction to an oxygen-rich environment ($K_2S_2O_8$ solution), the Mo^{5+} is reoxidized to Mo^{6+}, causing the MoO_3 nanoparticles to revert to their original pale-yellow state. XPS measurement was used to characterize the valence changes of Mo atoms (Figure S14), showing the content changes in Mo^{6+} and Mo^{5+} of the SAME-PCFs before and after UV irradiation. After UV irradiation, the content of Mo^{5+} increases slightly because some Mo^{6+} are transferred to Mo^{5+} when they get an electron from their surroundings.

$$MoO_3 + hv \rightarrow MoO_{3*} + e^- + h^+ \quad (1)$$

$$2h^+ + H_2O \rightarrow 2H^+ + O \quad (2)$$

$$MoO_3 + xe^- + xH^+ \rightarrow H_xMo_xM_{1-x}^{IV}O_3 \quad (3)$$

$$Mo^{6+} + e^- \rightarrow Mo^{5+} \quad (4)$$

$$hv + Mo_A^{5+} + Mo_8^{6+} \rightarrow Mo_A^{6+} + Mo_8^{5+} \quad (5)$$

The photochromic performances of SAME-PCF, including coloration intensity, response time, retention time, and color difference (ΔE), were then measured and assessed using a UV–vis spectrophotometer. Figure 4B shows a broad absorption band near 760 nm, attributable to the reduction of Mo^{6+} to Mo^{5+} [33]. The absorption intensity of SAME-PCF at a wavelength of 760 nm increases from approximately 0.01 to 1.23 with increasing UV dose until it reaches a saturation point at a UV dose of 48 kJ m^{-2}. This is accompanied by a noticeable shift in the color of the SAME-PCF from pale yellow to blue following exposure to UV light (Figure 4c). The images in Figure S15 display the alteration in color of SAME-PCF as the UV irradiation time increases. Then, the absorption intensity of SAME-PCF undergoes an obvious decline after treatment with a 0.5% $K_2S_2O_8$ solution at a temperature of 80°C. The value diminishes from around 1.2 to 0

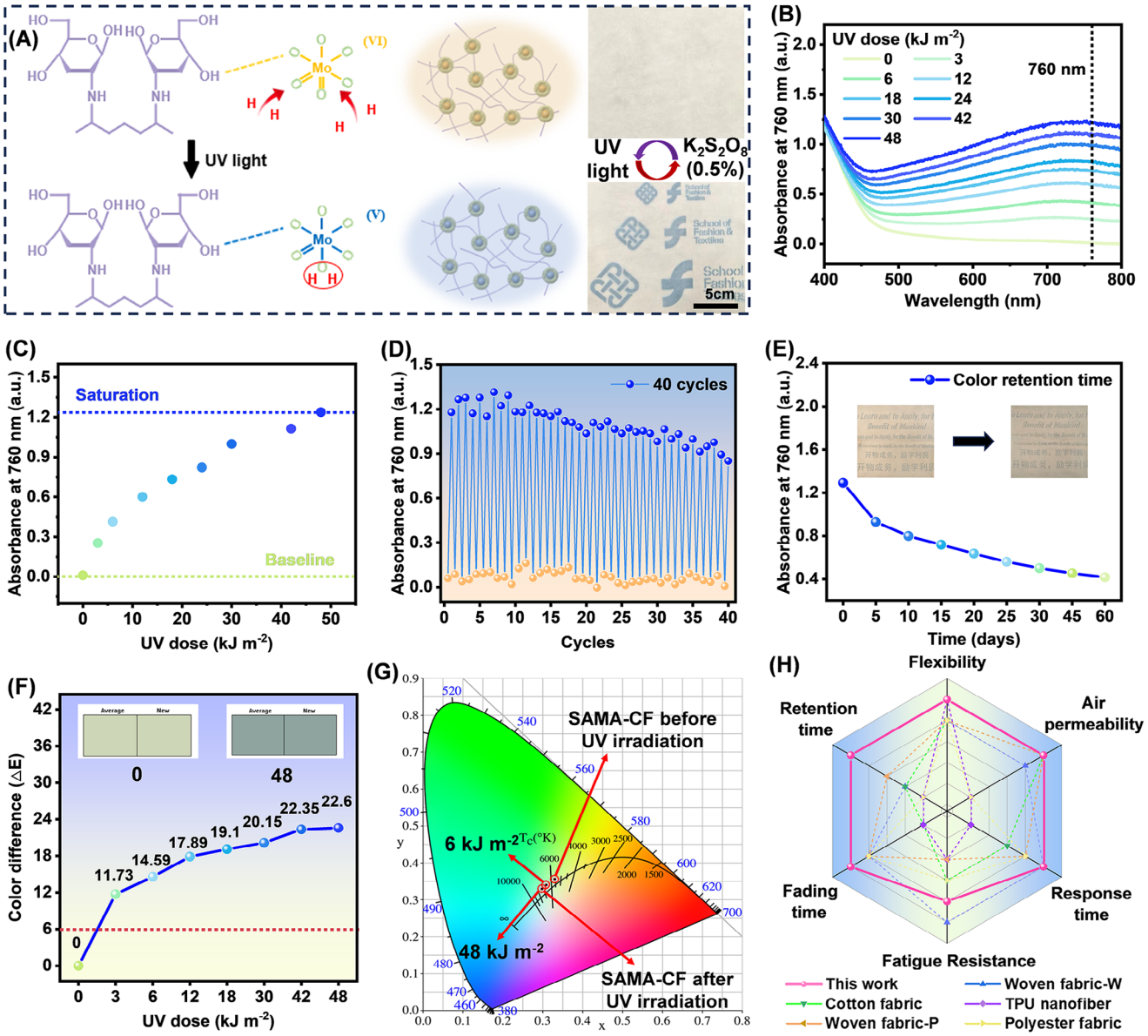

FIGURE 4 | Photochromic mechanism and performances of the SAME-PCFs. (A) Photochromic reaction mechanism of SAME-PCFs. (B) UV–vis absorbance spectra of the SAME-PCFs with increasing exposure to UV light ($\lambda = 365$ nm). (C) Absorbance at 760 nm as a function of UV dose for the SAME-PCFs. (D) Absorption intensity represents the fatigue resistance of the SAME-PCFs switching color from pale yellow to blue. (E) The change in UV–vis absorbance at 760 nm indicates the retention time of the SAME-PCFs in 60 days. (F) Color difference (ΔE) of the SAME-PCFs with increasing UV dose via Macbeth Color-Eye 7000 A under CIE standard illuminant D65 and 10° standard chromaticity. (G) CIE coordinate diagrams of pristine cotton fabric and the SAME-PCFs before and after UV irradiation in the (x, y) chromaticity diagram. (H) Comparison of the performances between various photochromic wearables.

as treatment duration extends, attaining a plateau at 600 s (Figure S16). Concurrently, the SAME-PCFs returned to their original pale-yellow state.

In the production of wearable photochromic fabrics, it is essential to assess their fatigue resistance and color retention duration [14]. Figure 4D illustrates the fatigue resistance of the photochromic wearables by quantifying the absorbance levels in both colored and bleached conditions. The absorption intensity of SAME-PCFs at a wavelength of 760 nm shows a slight decrease from around 1.2 to 0.85 after 40 cycles, suggesting that SAME-PCFs possess exceptional fatigue resistance and offer considerable potential in customizable photo-patterning information storage/recording. Figure 4E illustrates that the absorbance of SAME-PCFs diminishes from around 1.2 to 0.41 over 60 days, indicating that SAME-PCFs exhibit remarkable color retention. The SAME-PCFs demonstrate one of the longest color retention durations among all reported photochromic textiles. The exceptional fatigue resistance and prolonged color retention indicate that the SAME-PCFs have significant practical application potential in sustainable, long-lasting, and efficient customizable photo-patterning textiles. ΔE and chromaticity are additionally quantified to demonstrate the coloration intensity of SAME-PCFs. The color variation in Figure 4F demonstrates that the SAME-PCFs undergo a

significant color transformation during the photochromic process. At a UV dosage of 3 kJ m^{-2}, the ΔE is 11.73 ($\Delta E > 6$). The ΔE then escalates to 22.6 as the UV dose is augmented to 48 kJ m^{-2}. Furthermore, elevated UV exposure results in a consistent reduction in the reflectance of the SAME-PCFs (Figure S17). Figure 4G depicts the CIE 1931 chromaticity diagram of the PCF and SAME-PCFs after exposure to UV irradiation. When exposed to 365 nm UV light with the UV dose of 6 and 48 kJ m^{-2}, the SAME-PCFs' coordinates are far distant from the PCF, revealing an apparent color gap. Compared with existing photochromic fabrics, SAME-PCFs demonstrate comprehensive advantages, including excellent flexibility, superior air permeability, great fatigue resistance, great color retention time, short fading time, and fast response time (Figure 4H; Tables S1 and S2, and Note S1).

Photochromic wearables frequently encounter diverse environmental alterations, including pH variations and laundering, during everyday use; thus, assessing their stability in intricate and dynamic conditions is crucial. Because MoO_3 is an acidic oxide, it takes part in a neutralization reaction in alkaline conditions that makes molybdate and water. Detergents like alkaline solutions (pH > 8) can entirely eradicate the photochromic properties of MoO_3. MoO_3 nanoparticles can be contained within a small area of chitosan by encasing them in chitosan and SA. This can protect them from damage from the outside, such as acidic and alkaline solutions and washing. Figure 5A shows that chitosan surrounds MoO_3 nanoparticles, and MM nanoparticles treated with SA can easily and quickly change colors when exposed to UV light and a $K_2S_2O_8$ solution. The images of the MoO_3 and MM nanoparticles are shown in Figure 5B. Compared to the MoO_3 nanoparticles (Figure $5b_i$), the MM nanoparticles possess a coarse and uneven surface that is similar to a polymer wrinkle (Figure $5b_{ii}$). This shows that the MM nanoparticles form a shell-core structure with MoO_3 nanoparticles as the core and chitosan as the shell. We show a schematic diagram of the acid- and alkali-resistant photochromic wearable system in Figure 5C to show how stable SAME-PCFs are in complex environments. It reveals that the chitosan and SA network act as a protective barrier for the MoO_3 nanoparticles, enabling smooth color switching of the SAME-PCFs with the use of $K_2S_2O_8$ solution and preventing any negative impact of the chemical reaction caused by acid solution and alkaline laundry detergent. The XRD profiles of SAME-PCFs show the same diffraction patterns before and after washing (Figure 5D), verifying that the washing process did not change the structure of the materials. We then assessed the photochromic performance of SAME-PCFs using a UV–vis spectrophotometer after washing. As shown in Figure 5E, the absorption intensity of SAME-PCFs at a wavelength of 760 nm shows a modest decline from approximately 1.3 to 0.85 after undergoing 15 cycles of washing. Figure 5F illustrates that the absorbance value of SAME-PCFs is approximately 0.85 following a repeated pattern over 10 cycles after washing, while Figure S18 indicates that the absorbance of SAME-PCFs diminishes from roughly 0.85 to 0.39 in 30 days after washing. The SAME-PCFs exhibit excellent washing fastness, which is essential for routine soaking and laundering with detergent. In addition, this photochromic fabric has exceptional stability over a range of pH settings (pH 2–9). Figure 5G,H, exhibit that the UV absorbance of SAME-PCF treated with the acid and artificial sweat solution remains stable, and Figure 5I shows the UV absorbance of SAME-PCF treated with the alkali solution shows a relative decrease. This demonstrates that the strong encapsulation of MoO_3 by chitosan and SA enables the SAME-PCFs to maintain their outstanding photochromic performance even when the pH level changes. The exceptional washing fastness and remarkable environmental stability indicate that the SAME-PCFs have significant practical application potential in sustainable, long-term, efficient, and stable photo-patterning fabrics, even under adverse conditions. The high fatigue resistance, great washing fastness, and excellent stability suggest that the SAME-PCFs have considerable practical application potential in customizable patterns, sustainable and information security encryption, and even in harsh situations.

The stability of photochromic fabric across a broad temperature range and its insensitivity to sun radiation guarantee that the designs on the fabric remain distinct throughout several seasons for prolonged outdoor use and athletic endeavors. Figure 6A reveals the SAME-PCFs have stable photochromic properties during temperature variations between −30°C and 60°C, which is attributed to the excellent thermal stability of the MoO_3 nanoparticles. Figure 6B illustrates that the absorption intensity of SAME-PCFs rises to around 0.3 at a wavelength of 760 nm following 1 day of indoor light exposure, without compromising the clarity of the fabric pattern. Figure 6C shows that the absorption intensity of the unoccupied area on the SAME-PCFs rises to about 0.45 after sunlight exposure for 6 h (a UV index of 7175 mW m^{-2}). These demonstrate that the SAME-PCF can maintain distinct patterns during prolonged indoor illumination and solar exposure. We have conducted experiments on customizable patterns of SAME-PCFs for rewritable image data. The SAME-PCFs demonstrate the inscription and removal of distinctly recognizable patterns, such as a plane, snowman, bus, and fork (Figure 6D). The printed designs are easily removable and maintain their visibility in environmental conditions for at least 60 days. Furthermore, Figure S19 shows the writing–erasing cycles of 400 cm^2 SAME-PCFs that were done 10 times. This shows that SAME-PCFs can be easily used for scalable, customizable pattern applications. Figure 6E illustrates that the rewritable T-shirt (Figure $6E_i$), manufactured using the same production technique, possesses the capability to customize patterns. The patterns can be removed using an aqueous $K_2S_2O_8$ solution at 80°C, restoring the SAME-PCF T-shirt to its original pale-yellow state for subsequent UV printing, allowing the rewritable T-shirt to be adorned with various designs. After UV irradiation with a customized mask, the clearly identifiable pattern can be easily printed on the SAME-PCFT shirt (Figure $6E_{ii}$). The pattern can be erased, and other patterns can be printed by UV irradiation (Figure $6E_{iii}$). Figure $6E_{iv}$ shows the photos of volunteers wearing clothes, and the patterns are clearly visible. Furthermore, the exceptional stability and durability guarantee the longevity of the SAME-PCF T-shirt under typical wear and usage conditions. To execute SAME-PCFs' information storage and encryption capabilities, the image depicted in Figure 5C was encoded and stored within a QR code. When a UV lamp was used to shine on the skeletonized QR code mask, a clear QR code showed up on the surface of the SAME-PCFs, with a resolution of about 1 mm (Figure 6F). Mobile phones can swiftly identify the QR code and direct users to the webpage featuring Figure 5C. This demonstrates that SAME-PCFs have considerable potential for use in anti-counterfeiting marks and information security encryption.

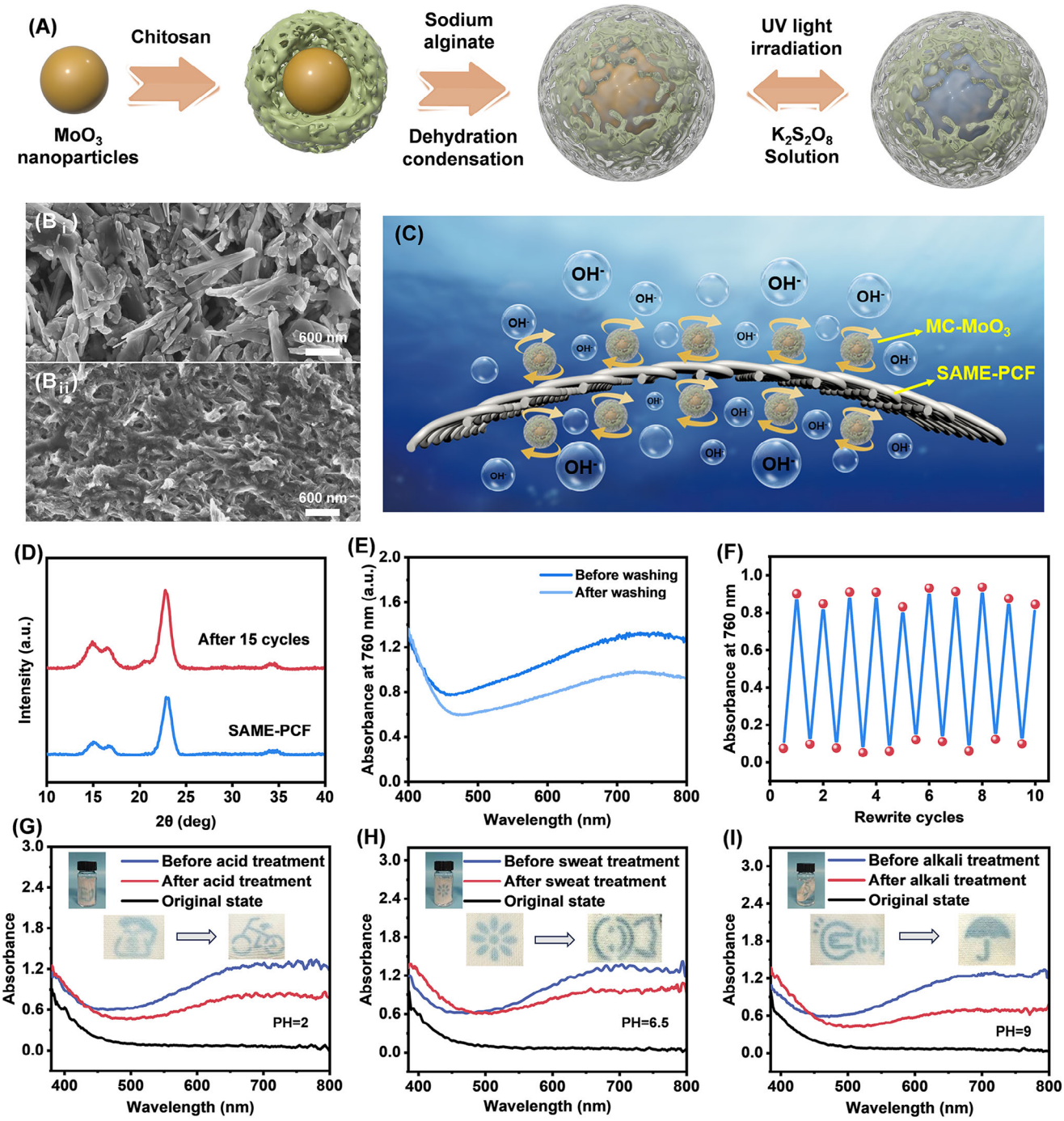

FIGURE 5 | Stability of photochromic performances of the SAME-PCFs. (A) Schematic diagram of MoO_3 nanoparticles encapsulated by chitosan and SA. SEM images of the (B_i) MoO_3 nanoparticles and (B_{ii}) MM nanoparticles. (C) Illustration of SAME-PCFs showing great stability in facing varying pH environments. (D) x-Ray diffraction patterns of SAME-PCFs before and after washing. (E) The UV–Vis absorbance spectra of SAME-PCFs with UV irradiation of 48 kJ m^{-2} after washing. (F) Absorption intensity represents the fatigue resistance of the SAME-PCFs after washing. (G) The change in absorbance of SAME-PCFs after acid treatment. (H) The change in absorbance of SAME-PCFs after sweat treatment. (I) The change in absorbance of SAME-PCFs after alkali treatment.

3 | Conclusion

In summary, we design and employ a scalable technology for developing by integrating the MM nanoparticles with sheath-core structure into PCFs through covalent bonds and combing MM nanoparticles with SA by electrostatic force and peptide linkage. The prepared photochromic fabric shows reversible color conversion from pale yellow to blue under exposure to UV light and $K_2S_2O_8$ solution. The SAME-PCF possesses excellent photochromic performance, including great fatigue resistance (>40 cycles), fast light response reaching color saturation with a UV dose of 48 kJ m^{-2}, and superior color retention time (>60 days). Owing to the encapsulation of chitosan and SA for MoO_3 nanoparticles, the photochromic wearable has great stability in

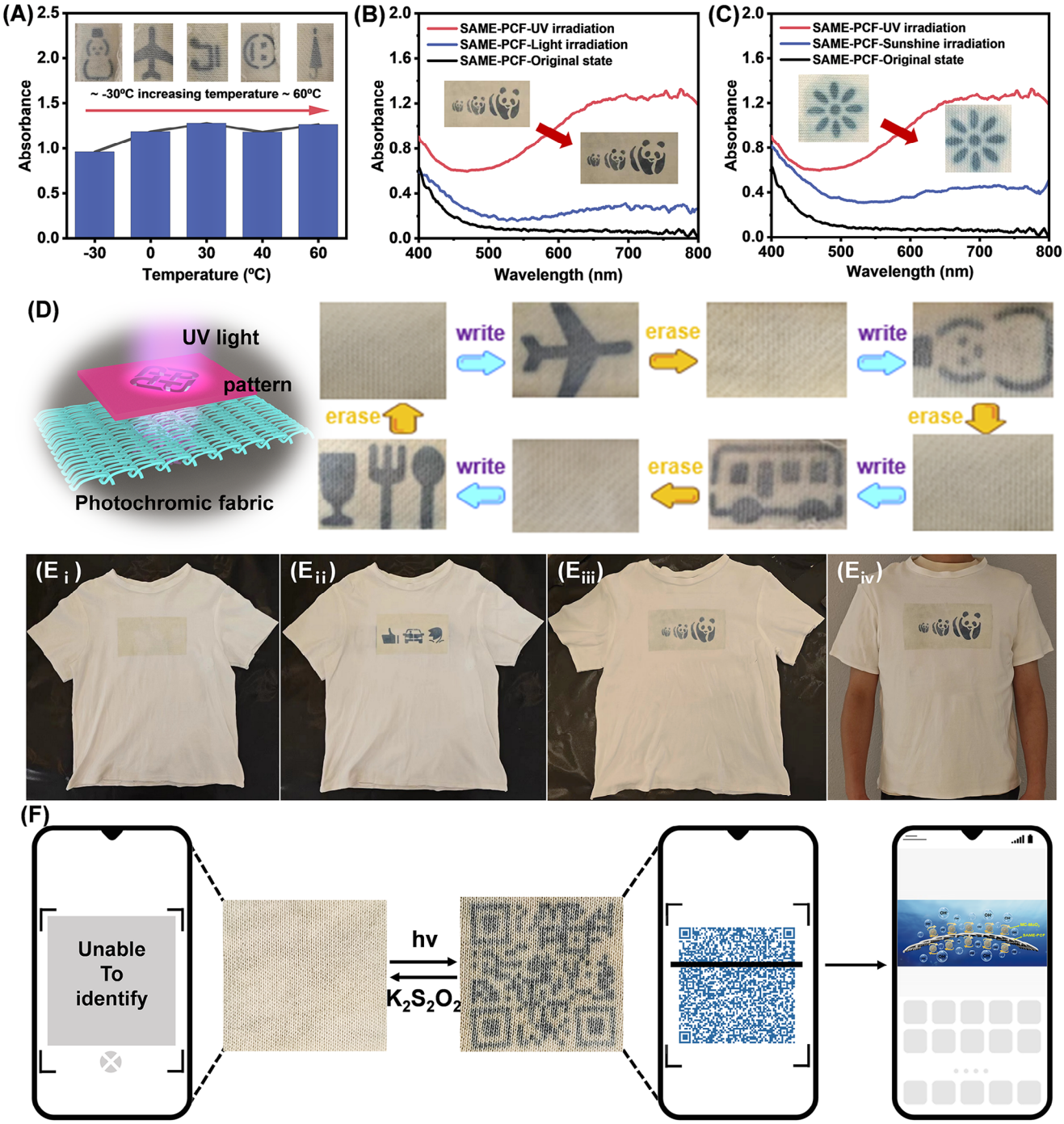

FIGURE 6 | Practical application of SAME-PCFs. (A) The absorbance change of SAME-PCFs at various temperatures. (B) The absorbance of SAME-PCFs under the indoor light. (C) The absorbance of SAME-PCFs under the sunshine. (D) Images showing the customizable patterns of SAME-PCFs for rewritable image data. (E) Images displaying the volunteer wearing the photochromic textile with different patterns. (F) Application of SAME-PCFs in QR code information security encryption system.

various harsh environments such as acid solution, alkali solution, sweat (pH 2.0–9.0), indoor and sunshine irradiation, and sustains repeated washing. Moreover, this photochromic fabric exhibits great wearability with excellent flexibility of 17 mm and biocompatibility (cell viability > 95%). These characterizations promote it as a promising choice for daily wear and sports. Besides, a rewritable T-shirt and a QR code information security encryption system by the SAME-PCFs have been presented, demonstrating its potential in the domains of customizable patterns, flexible rewritable textiles, and information security encryption. In particular, this concept of using encapsulation technology to endow MoO_3 nanoparticles with durability and stability for the creation of MoO_3-based photochromic dyes can be extensively applied to photochromic wearables. It paves a new route for achieving scalable, sensitive light response, environmental stability, and color-retaining photochromic textiles in the field of customizable pattern recording/storage, smart textiles, and information security encryption.

4 | Experimental Section

4.1 | Materials

Cotton fabric was purchased from Suqian Fina Trading Co. Ltd., China. Sodium molybdate (Na_2MoO_4) was provided by Shanghai Macklin Biochemical Technology Co. Ltd. Ethylene diamine tetraacetic acid (EDTA) and KH560 were obtained from Shanghai Aladdin Biochemical Technology Co. Ltd., China. Chitosan, Tween 80, GA solution 25%, acetic acid, sodium hydroxide (NaOH), petroleum ether, SA, ethanol alcohol, hydrochloric acid (HCl, 38%), sodium bicarbonate ($NaHCO_3$), sodium chloroacetate, acetone, and $K_2S_2O_8$ were purchased from DIECKMANN. Artificial sweat was bought from Shenzhen Zhongwei Instrument Equipment Co. Ltd., China.

4.2 | Preparation of MM Nanoparticles

To prepare MoO_3 nanoparticles, a predetermined quantity of Na_2MoO_4 was dissolved in 50 mL of deionized water to form a solution with a concentration of 0.1 mol L^{-1}. Afterwards, a saturated solution of EDTA was introduced into this mixture while stirring constantly at room temperature. The pH of the solution was subsequently modified to 1.5 using HCl, while the combination was stirred in the absence of light for a duration of 4 h. Subsequently, the solution was put into a 100-mL autoclave and exposed to hydrothermal treatment at a temperature of 120°C for 48 h. Following the treatment, the light blue MoO_3 nanoparticles were gathered and underwent multiple washes using distilled water and ethanol alcohol to eliminate any contaminants. After that, the MoO_3 nanoparticles were evenly distributed in a 200-mL solution of 0.3% acetic acid, which was mixed with 1.2 g of chitosan and 4 g of Tween 80. Next, the mixture was subjected to ultrasonic treatment for 3 h, and then the cell grinder was used to grind the mixture for 30 min. Afterwards, a 4 mL solution of GA was dropped and constantly stirred for 4 h to chemically bond the chitosan and solidify the microcapsule. The MM nanoparticles were ultimately centrifuged and washed with petroleum ether with a volume percentage of 30%.

4.3 | Preparation of SAME-PCF

Initially, the knitted cotton fabrics were treated with a 20 g L^{-1} NaOH solution to remove oil and impurities and enhance the presence of additional functional groups on the fiber surface. Next, cotton fabrics were immersed in a solution of KH-560 with a concentration of 1.5% at a temperature of 60°C for 12 h. The fabrics were then cleaned using acetone and distilled water, resulting in the production of the E-PCFs. After the treatment, place the treated fabrics at 60°C to dry for 4 h. Afterwards, separately prepare a solution of MM nanoparticles (with concentrations ranging from 5–20 mg mL^{-1}) and a solution of SA (5 mg mL^{-1}). The pH values of both solutions were adjusted to 5. Subsequently, the E-PCFs were immersed in a solution of MM nanoparticles for 4 h. They were then dried at a temperature of 60°C for 4 h, resulting in the formation of the ME-PCFs. Afterwards, the ME-PCFs were submerged in a solution of the SA for 30 min and subsequently subjected to a drying process at a temperature of 60°C for 4 h. Ultimately, this procedure needs to be replicated 1–4 times in order to prepare the SAME-PCF.

4.4 | Characterization

The surface morphology of these fabrics, MoO_3 nanoparticles, and MM nanoparticles was investigated by scanning electron microscopy (SEM). The morphology of MoO_3 nanoparticles was examined using a transmission electron microscope (TEM). The XRD technique was used to study the crystal structure and phase composition of the MoO_3 nanoparticles and functionalized fabrics. XPS (Kratos Axis 165) was used to examine the valence changes of Mo atoms. The structure of the PCF, E-PCF, ME-PCF, and SAME-PCF was analyzed using Fourier transform infrared spectroscopy (FT-IR). The mechanical properties of the samples were evaluated using a universal material testing machine (3365, Instron, USA). The contact angle measurement equipment (SDC-350) was used to quantify the hydrophilicity of the textiles. The elemental composition and distribution of the samples were examined by using energy-dispersive x-ray spectroscopy (EDS) mapping. The content of the PCF, E-PCF, ME-PCF, and SAME-PCF was measured by thermogravimetric analysis (TGA). An MO21S air permeability tester (KES, Kato Tech Co. Ltd.) was used to measure the air permeability (mm s^{-1}) of fabrics depending on the ASTM D737-08 standard. The washing ability of photochromic fabrics was assessed in accordance with the AATCC TM 135–2004 standard. The UV–vis absorption spectra of the samples were measured using a UV–vis spectrophotometer (Agilent Cary 300 Conc). The ΔE and CIE coordinate diagrams of photochromic fabrics were assessed using the Macbeth Color-Eye 7000 A (Dearly Enterprise Ltd., China) under the CIE standard illuminant D65 and 10° standard chromaticity. The cytotoxicity of photochromic fabrics was assessed using L-929 cells (ATCC, US) by the CCK-8 assay.

Acknowledgments

This work was supported by the Innovation and Technology Commission of the Government of the Hong Kong Special Administrative Region (Project No. ITS/139/21), and J. Zhang would like to thank The Hong Kong Polytechnic University for providing him with a postgraduate scholarship.

Conflicts of Interest

The authors declare no conflicts of interest.

References

1. J. Lu, H. Fu, X. Tian, Y. Chen, and B. Xu, "Advanced Design of Organic Ionic Materials for the Boost of Electricity Generation, Storage, and Utilization," *Advanced Energy Materials* 14, no. 43 (2024): 2402130.

2. J. Zhang, J. Liu, Z. Zhao, et al., "Calotropis Gigantea Fiber-Based Sensitivity-Tunable Strain Sensors With Insensitive Response to Wearable Microclimate Changes," *Advanced Fiber Materials* 5, no. 4 (2023): 1378–1391.

3. J. Lu, B. Xu, J. Huang, X. Liu, and H. Fu, "Charge Transfer and Ion Occupation Induced Ultra-Durable and All-Weather Energy Generation From Ambient Air for Over 200 Days," *Advanced Functional Materials* 34, no. 42 (2024): 2406901.

4. J. Zhang, B. Xu, K. Chen, et al., "Revolutionizing Digital Healthcare Networks With Wearable Strain Sensors Using Sustainable Fibers," *SusMat* 4, no. 4 (2024): e207.

5. Z. Wang, Y. Bo, P. Bai, et al., "Self-Sustaining Personal All-Day Thermoregulatory Clothing Using Only Sunlight," *Science* 382, no. 6676 (2023): 1291–1296.

6. J. Qian, Q. Dong, K. Chun, et al., "Highly Stable, Antiviral, Antibacterial Cotton Textiles via Molecular Engineering," *Nature Nanotechnology* 18, no. 2 (2023): 168–176.

7. T. Ahmed, Y. Gao, M. Y. So, et al., "Diamond-Structured Fabric-Based Triboelectric Nanogenerators for Energy Harvesting and Healthcare Application," *Advanced Functional Materials* 34, no. 48 (2024): 2408680.

8. T. Chen, B. Xu, J. Han, et al., "Chelating Coordination Regulated Photochromic Electrospun Nanofibers for Waterproof and Long-Color-Retention Rewritable Wearables," *ACS Applied Materials & Interfaces* 16, no. 10 (2024): 13305–13315.

9. M. Zhu, B. Xu, T. Chen, J. Zhang, and W. Sun, "Advanced Functional Photochromic Wearables With Superior Durability and Stability for Sustainable Applications," *Advanced Functional Materials*, no. 42 (2024): 2406840.

10. J. Zhang, T. Chen, M. Zhu, et al., "Scalable, Fast Light-Responsive, and Excellent Color-Retention Fiber-Based Photochromic Wearables for Sustainable Photo-Patterning and Information Security Encryption," *Advanced Functional Materials* (2024): 2415622.

11. R. Pardo, M. Zayat, and D. Levy, "Photochromic Organic-Inorganic Hybrid Materials," *Chemical Society Reviews* 40, no. 2 (2011): 672–687.

12. J. Zhang, Q. Zou, and H. Tian, "Photochromic Materials: More Than Meets the Eye," *Advanced Materials* 25, no. 3 (2013): 378–399.

13. G. Xi, L. Sheng, J. Du, et al., "Water Assisted Biomimetic Synergistic Process and Its Application in Water-Jet Rewritable Paper," *Nature Communications* 9, no. 1 (2018): 4819.

14. J. Li, Y. Liu, Z. Gu, et al., "Scalable, Green, Flexible Photochromic Bacterial Cellulose for Multicolor Switching, Photo-Patterning, and Daily Sunlight UV Monitoring," *Small* 20, no. 30 (2024): 2309514.

15. P. K. Kundu, D. Samanta, R. Leizrowice, et al., "Light-Controlled Self-Assembly of Non-Photoresponsive Nanoparticles," *Nature Chemistry* 7, no. 8 (2015): 646–652.

16. P. Liu, B. Wang, C. Wang, et al., "Amorphous Tungsten Oxide Nanodots for Chromatic Applications," *Advanced Functional Materials* 34, no. 34 (2024): 2400760.

17. S. Kawata and Y. Kawata, "Three-Dimensional Optical Data Storage Using Photochromic Materials," *Chemical Reviews* 100, no. 5 (2000): 1777–1788.

18. D. K. Macharia, S. Sarker, B. Zhu, et al., "Constructing On-Demand Photoreversible Mono/Multi-Color Switching Fabrics With Plasmonic In-Doped ZnO Catalyzed Systems," *Chemical Engineering Journal* 425 (2021): 130638.

19. T. Chen, B. Xu, M. Zhu, et al., "Advanced Functional Photochromic Wearables With Fast Photo-Responsivity, Long Color-Retention, and Multi-Environmental Stability," *Chemical Engineering Journal* 490 (2024): 151804.

20. M. Yang, Q. Han, X. Liu, et al., "Ultrahigh Stability 3D TI Bi_2Se_3/MoO_3 Thin Film Heterojunction Infrared Photodetector at Optical Communication Waveband," *Advanced Functional Materials* 30, no. 12 (2020): 1909659.

21. B. Qin, H. Chen, H. Liang, et al., "Reversible Photoswitchable Fluorescence in Thin Films of Inorganic Nanoparticle and Polyoxometalate Assemblies," *Journal of the American Chemical Society* 132, no. 9 (2010): 2886–2888.

22. A. De CastroI, R. S. Datta, J. Z. Ou, et al., "Molybdenum Oxides—From Fundamentals to Functionality," *Advanced Materials* 29, no. 40 (2017): 1701619.

23. J. Liu, S. Shao, G. Fang, et al., "High-Efficiency Inverted Polymer Solar Cells With Transparent and Work-Function Tunable MoO_3-Al Composite Film as Cathode Buffer Layer," *Advanced Materials* 24, no. 20 (2012): 2774–2779.

24. H. Kanno, R. J. Holmes, Y. Sun, S. Kena-Cohen, and S. R. Forrest, "White Stacked Electrophosphorescent Organic Light-Emitting Devices Employing MoO_3 as a Charge-Generation Layer," *Advanced Materials* 18, no. 3 (2006): 339–342.

25. A. El Kadib, "Chitosan as a Sustainable Organocatalyst: A Concise Overview," *ChemSusChem* 8, no. 2 (2015): 217–244.

26. H. Amiri, M. Aghbashlo, M. Sharma, et al., "Chitin and Chitosan Derived From Crustacean Waste Valorization Streams Can Support Food Systems and the UN Sustainable Development Goals," *Nature Food* 3, no. 10 (2022): 822–828.

27. S. Mura, J. Nicolas, and P. Couvreur, "Stimuli-Responsive Nanocarriers for Drug Delivery," *Nature Materials* 12, no. 11 (2013): 991–1003.

28. Y. B. Miao, Y. J. Lin, K. H. Chen, et al., "Engineering Nano-and Microparticles as Oral Delivery Vehicles to Promote Intestinal Lymphatic Drug Transport," *Advanced Materials* 33, no. 51 (2021): 2104139.

29. Z. Ma, Z. Yang, Q. Gao, et al., "Bioinspired Tough Gel Sheath for Robust and Versatile Surface Functionalization," *Science Advances* 7, no. 15 (2021): eabc3012.

30. O. Lupan, V. Trofim, V. Cretu, et al., "Investigation of Optical Properties and Electronic Transitions in Bulk and Nano-Microribbons of Molybdenum Trioxide," *Journal of Physics D: Applied Physics* 47, no. 8 (2014): 085302.

31. M. Yan, Y. Shen, L. Zhao, and Z. Li, "Synthesis and Photochromic Properties of EDTA-Induced MoO_3 Powder," *Materials Research Bulletin* 46, no. 10 (2011): 1648–1653.

32. J. Fan, B. Bao, Z. Wang, et al., "Flexible, Switchable and Wearable Image Storage Device Based on Light Responsive Textiles," *Chemical Engineering Journal* 404 (2021): 126488.

33. E. Papaconstantinou, "Photochemistry of Polyoxometallates of Molybdenum and Tungsten and/or Vanadium," *Chemical Society Reviews* 18 (1989): 1–31.

Supporting Information

Additional supporting information can be found online in the Supporting Information section.

Supporting Information